HHS Public Access

Author manuscript

Anal Chem. Author manuscript; available in PMC 2018 September 05.

Published in final edited form as:

Anal Chem. 2017 September 05; 89(17): 9601–9608. doi:10.1021/acs.analchem.7b02933.

Critical comparison of FRET-sensor functionality in the cytosol and endoplasmic reticulum and implications for quantification of ions

Kyle P. Carter[#1,2], **Margaret C. Carpenter**[#1,2], **Brett Fiedler**[1,3], **Ralph Jimenez**[1,3], and **Amy E. Palmer**[1,2,*]

[1]Department of Chemistry and Biochemistry, University of Colorado Boulder, CO 80303

[2]BioFrontiers Institute, University of Colorado, Boulder, CO 80303

[3]JILA/NIST, University of Colorado and National Institute of Standards and Technology, Boulder, CO 80309

[#] These authors contributed equally to this work.

Abstract

Genetically-encoded sensors based on fluorescence resonance energy transfer (FRET) are powerful tools for quantifying and visualizing analytes in living cells, and when targeted to organelles have the potential to define distribution of analytes in different parts of the cell. However, quantitative estimates of analyte distribution require rigorous and systematic analysis of sensor functionality in different locations. In this work, we establish methods to critically evaluate sensor performance in different organelles and carry out a side-by-side comparison of three different genetically encoded sensor platforms for quantifying cellular zinc ions (Zn^{2+}). Calibration conditions are optimized for high dynamic range and stable FRET signals. Using a combination of single-cell microscopy and a novel microfluidic platform capable of screening thousands of cells in a few hours, we observe differential performance of these sensors in the cytosol compared to the ER of HeLa cells, and identify the formation of oxidative oligomers of the sensors in the ER. Finally, we use new methodology to re-evaluate the binding parameters of these sensors both in the test tube and in living cells. Ultimately, we demonstrate that sensor responses can be affected by different cellular environments, and provide a framework for evaluating future generations of organelle-targeted sensors.

[*]To whom correspondence should be addressed Amy.Palmer@colorado.edu.

ASSOCIATED CONTENT

Supporting Information Available: This material is available free of charge via the Internet.
Figures S1–13 and Tables S1–6

Author Contributions

The manuscript was written through contributions of all authors. All authors have given approval to the final version of the manuscript.

Notes

The authors declare no competing financial interest.

INTRODUCTION

Fluorescent sensors are powerful tools for visualizing and quantifying ions, metabolites, and other species in cells, offering the potential to define the concentration and spatial distribution of such species. But realizing this potential requires systematic and careful characterization of sensor platforms in the complex environment of a living cell and in different subcellular locations. The need for a robust analytical framework for comparing sensor performance and defining sensor functionality in different cellular locations is illustrated by comparing the three families of genetically-encoded FRET-based sensors, Zap, eCALWY, and eZinCh, which have been applied to define Zn^{2+} pools within the cell. Each family is engineered by fusing fluorescent proteins (FP) to Zn^{2+} responsive protein domains. The Zap family links a donor CFP to an acceptor citrine YFP through the zinc-binding domain of the yeast transcription factor Zap1.[1] In the eCALWY family of sensors, cerulean FP and citrine YFP were mutated to recognize each other in the apo state of the sensor, and the metal-binding domains of Atox1 and WD4 were engineered to coordinate Zn^{2+}.[2] In the eZinCh family a Zn^{2+} coordination site was directly engineered into an interface between the β-barrels of cerulean and citrine, which were connected by a flexible linker.[3] A notable benefit of genetically-encoded sensors is that they can be targeted to organelles by fusing small peptide signaling sequences to the sensors. Members of these families of sensors have been targeted to different cellular compartments including: cytoplasm, mitochondria, Golgi apparatus, nucleus, and endoplasmic reticulum.[1,3–6] Application of multiple platforms for measuring analytes in cells can increase confidence in the robustness of both the tools and their measurements. These three sensor platforms have been used in the cytosol to estimate labile Zn^{2+} within an order of magnitude, 82–600 pM.[7,8] In contrast, when the same sensors were targeted to the ER of HeLa cells the estimates of labile Zn^{2+} ranged widely from 0.9–1600 pM.[1,3,6] Qualitatively, ZapCY1 is more saturated in the cytosol than in the ER, while eCALWY-4 displays the opposite saturation pattern and eZinCh-2 is about equally saturated in both the ER and the cytosol.[1,3,6] It's possible the chemical environment of the ER (pH, crowding, or redox state) differentially affects sensors, impacting sensor functionality and accuracy of quantifications. Defining whether the labile Zn^{2+} concentration is higher in the ER than in the cytosol is an important fundamental question in Zn^{2+} biology in order to establish whether the ER might serve as a store of Zn^{2+} that could be mobilized for cellular signaling. More generally, establishing a framework for comparing different sensor platforms and establishing performance metrics in organelles compared to the cytosol may be important for sensors of other analytes such as Ca^{2+}, Mg^{2+}, or other metal ions.

In this work, we establish a framework for critically comparing ratiometric FRET-based sensors in an organelle of interest by comparing ZapCY1, eCALWY-4, and eZinCh-2 in the ER and cytosol of HeLa cells. We had two main goals in this study: first, outline methods to systematically assess sensor performance, and second, shed light on relative Zn^{2+} levels in the cytosol and ER. We show that calibrations must be optimized to obtain accurate quantification of analytes, and that sensors can perform very differently in the cytosol versus organelles. We applied recently developed microfluidic technology to screen the response of localized sensors to Zn^{2+} over thousands of cells to ensure the trends observed in tens of representative cells hold over large populations[9]. Additionally, we reevaluated the K_d of the

sensors *in vitro* and compared to *in situ* titrations of the sensors in the ER to better understand how the environment of the ER affects Zn^{2+} binding. Taken together the data indicate that the ER of HeLa cells is depleted of labile Zn^{2+} compared to the cytosol.

RESULTS AND DISCUSSION

Identifying Optimal Calibration Conditions.

Accurate calibration of sensor response is essential for using sensors to estimate analyte levels. Additionally, it is important to critically evaluate and identify optimal response conditions, which may differ in different cellular compartments. *In situ* calibration of Zn^{2+} sensors involves first measuring the FRET ratio (R) when the cell is at rest (R_{rest}). Next excess membrane-permeable Zn^{2+}-specific chelator, N,N,N′,N′-tetrakis (2-pyridylmethyl) ethylenediamine (TPEN), is added to measure the FRET ratio of the apo sensor (R_{apo}), followed by addition of excess Zn^{2+}, ionophores, and/or permeabilization reagents to measure the FRET ratio of Zn^{2+} replete sensor (R_{bound}). Stable and maximal sensor responses to the two extrema of Zn^{2+} concentrations are essential for accurately determining the resting saturation of the sensor.

To optimize one *in situ* calibration protocol that yielded saturating, stable R_{bound} responses of all three sensors in the ER and cytosol, we tested different concentrations of Zn^{2+}, pyrithione, and the inclusion of a membrane-permeabilizing agent, saponin. Our goal was to maximize the dynamic range and stability of the R_{bound} signal for each sensor (Supplementary Tables S1–2). As shown in Figure 1 and Supplementary Figure S1, under some calibration conditions, addition of saturating concentrations of Zn^{2+} led to an unstable signal characterized by an increase, followed by sharp decrease in the FRET ratio. To define the stability of the R_{bound} signal, we calculated the percent change in the R_{bound} signal over time (Supplementary Tables S1 and S2). We determined that addition of 2 nM buffered Zn^{2+}, 0.75 μM pyrithione, and 0.001% saponin led to large, stable responses of all three sensor platforms in both the cytosol and ER (Figure 1, Supplementary Figure S1, Supplementary Tables S1 and S2). Increased concentrations of pyrithione and Zn^{2+} or exclusion of saponin resulted in sub-optimal sensor responses that would lead to systematic error in estimated fractional saturation and Zn^{2+} concentrations. As shown in the subsequent section, achieving a stable R_{bound} was essential for clear estimation of sensor fractional saturation and dynamic range.

Fractional Saturation of the Sensors.

Using the new calibration conditions, each sensor was calibrated in both the ER and cytosol (Supplementary Figure S2) of HeLa cells. The stability of the FRET ratios and the maximal response of the sensors in each condition allow for clear quantification of the resting fractional saturation and dynamic range (defined as R_{bound}/R_{apo} for ZapCY1 and eZinCh-2 and R_{apo}/R_{bound} for eCALWY-4) of the sensors in the two cellular locations (Table 1). The fractional saturation describes the percent of sensor that is bound to Zn^{2+} under resting conditions in a particular organelle and is proportional to the concentration of labile Zn^{2+} such that higher fractional saturation suggests higher levels of labile Zn^{2+}. The dynamic range is the maximal change in signal upon Zn^{2+} binding and defines the sensitivity of a

sensor to small differences in Zn^{2+} concentration.[4,10] The data in Table 1 reveal that two sensor platforms (ZapCY1 and eCALWY-4) show decreased fractional saturation in the ER compared to cytosol, suggesting lower levels of Zn^{2+} in the ER compared to cytosol. One sensor platform (eZinCh-2) showed similar fractional saturation in both locations, but slighter higher saturation, suggesting higher Zn^{2+}, in the ER. However, it should be noted that the overall lower dynamic range of eZinCh-2 and eCALWY-4 in the ER compared to the cytosol makes them more prone to error.[4] Sensor calibrations under previously described conditions generally featured a lower dynamic range and rapidly changing, unstable R_{bound} signals, which could lead to erroneous estimation of fractional saturation (Supplementary Figure S3, Table S1–2). Given the agreement of ZapCY1 and eCALWY-4 sensors, coupled with the high dynamic range, the stability of the responses, and the consistency of the fractional saturation of ZapCY1, these results suggest that the concentration of labile Zn^{2+} in the ER is lower than in the cytosol.

High Throughput Measure of FRET Response.

A weakness of microscopy-based calibrations of FRET responses is that a limited number of cells can be assayed in any given experiment. We recently introduced a microfluidic cytometer capable of measuring FRET ratios for sensor states (R_{apo}, R_{bound}), as well as FRET changes in response to systematic addition of ligands within a defined time window from hundreds of ms up to 10 sec, in individual cells expressing sensors in a high throughput manner.[9,11] This cytometer permits measurement of variability in FRET states and FRET responses in thousands of cells to assess variability at the population-level. Here, we use this cytometer to compare cytosolic and ER-targeted sensors for all three sensor platforms. A distinct advantage of this platform is the ability to introduce reagents in a controlled manner that doesn't vary from cell to cell or experiment to experiment. However, one limitation is that the response time window is limited by device geometry and the pair matching algorithm[9]. Therefore, we only assess a sensor's ability to respond within a short time window (7.5 sec), which doesn't correspond to the full sensor response (Supplementary Figure S3 and S4). Given these considerations, we use the platform to define the initial FRET ratios and variability of ratios in the apo state, and examine the responsiveness of sensors upon addition of Zn^{2+}, as opposed to the magnitude of response (i.e. dynamic range), within the defined time window.

Figure 2a and 2b show histograms of single cell FRET populations at FRET 1 and FRET 2 for ER- and cytosol-targeted sensors, respectively. Since FRET populations did not exhibit a normal distribution, median based statistics were used to assess the center and heterogeneity of the cell populations. The robust coefficient of variation (RCV) was used to describe the width of the distribution, which serves as an indicator of the heterogeneity of a sensor in the apo state. The median and RCV values for each sensor in each compartment are presented in Supplementary Table S3. Comparison of these values for each sensor allowed us to define whether there were differences in the FRET state in different compartments. ZapCY1 showed similar RCV in the two locations (11.1% and 9.3% in ER and cytosol, respectively) suggesting comparable sensor heterogeneity, and a small, but significant shift in the median FRET 1 ratio when localized to the ER (1.01 versus 0.92 in the ER and cytosol, respectively). The eCALWY-4 sensor showed similarly broad FRET 1 distributions in the

ER and cytosol (22.8% and 26.5%, respectively), indicative of increased sensor heterogeneity in both locations compared to ZapCY1, and a significant shift in the median FRET ratio from 0.97 (ER) to 1.55 (cytosol). The eZinCh-2 sensor yielded the tightest FRET 1 distribution in the cytosol (RCV = 5.1%), indicating minimal heterogeneity, but the broadest distribution in the ER (RCV = 32.4%). For eZinCh-2 the FRET 1 median ratio shifted from 1.42 in the ER to 1.03 in the cytosol. Combined, these data reveal that localization to the ER can introduce significant heterogeneity into the apo state of a sensor.

This platform also enabled us to measure sensor responses to added analyte in a short time window and identify sub-populations of cells with sensors that are non-responsive sensor or that respond significantly differently than the average. Figure 2c and 2d show the pair-matched single cell response in the form of a histogram (FRET 2/ FRET 1), and the corresponding scattergram that illustrates the FRET change in individual cells (inset). All of the sensors gave rise to responsive populations (Figure 2c–d), but the overall shape of the scattergrams varies from sensor to sensor and is not univariate as the histograms may suggest. This is most exaggerated in ER-eCALWY-4 (Figure 2c, bottom panel), in which the histogram appears broad and unimodal, but the scattergram shows additional sub-populations indicating variability in the kinetics of the response from cell to cell. Comparison of scattergams for ER-targeted versus cytosolic sensors revealed a greater degree of heterogeneity in responsiveness for all ER sensors. While some of this heterogeneity may derive from increased variability in the apo FRET state, some may also arise from variable Zn^{2+} uptake kinetics in different cells. These studies reveal that all three sensor platforms are, to varying degrees, sensitive to some feature of the ER environment in a way that alters their response. Both the *in situ* calibration experiments and microfluidic analysis indicated that the response of all three sensors was diminished in the ER compared to the cytosol.

Analysis of Sensor Behavior in Cells.

To explore the possible origins of heterogeneity and diminished response in the ER sensor, localization and folding were analyzed by microscopy. Cells expressing ER-ZapCY1 or ER-eCALWY-4 exhibit fluorescence in a tubular network characteristic of the ER (Figure 3a–b). Many cells expressing ER-eZinCh-2 also have proper sensor localization (Figure 3c), but approximately 25% display bright puncta that are not typical of ER structure (Figure 3d), suggesting perturbation of the sensors themselves as well as ER morphology. Perturbation of ER structure by ER-eZinCh-2 occurred regardless of the localization signal used (Supplementary Figure S5).

Another possible explanation for the issues observed with ER-targeted sensors could be the formation of misfolded sensors or non-functional aggregates in the ER lumen. Fluorescent proteins have been shown to form disulfide-linked oligomers when expressed in the ER.[12] Additionally, all three sensors use Zn^{2+}-binding domains with cysteine residues that could potentially form aberrant disulfide bonds. Cells expressing ER-targeted Zn^{2+} sensors were analyzed by immunoblot to determine the degree of sensor oligomerization (Figure 3e). Under non-reducing conditions, all three sensors ran as high-molecular weight species that were not present under reducing conditions. The molecular weight of the higher-running

bands suggests the formation of dimers and trimers. These oligomers were not present when the sensors were expressed in the cytosol (Supplementary Figure S6a). While all three sensors oligomerize in the ER, the immunoblot analysis indicated that ER-eZinCh-2 was the most sensitive to oxidation. The extent of oxidation of ER-eZinCh-2 was not dependent on sensor concentration, as even cells with low levels of sensor expression displayed oxidative oligomers (Supplementary Figure S6b).

Taken together with microscopy images that reveal perturbation of ER morphology, these data indicate that eZinCh-2 is poorly suited to the oxidizing environment of the ER. The formation of oligomers may help explain the reduced dynamic range and variable FRET ratios of eZinCh-2 in the ER (Supplementary Table S1). The solvent-exposed, Zn^{2+}-binding cysteine residues engineered on the barrel of the fluorescent proteins in eZinCh-2 may be particularly susceptible to oxidation. The formation of intramolecular or intermolecular disulfide bonds between fluorescent proteins could lead to aggregated sensor molecules locked in a variety of FRET states. The oligomers detected by immunoblot may be related to the puncta observed in images of ER-eZinCh-2. However, it is possible that the oligomers formed by these sensors are not always readily detected by imaging.

In vitro Characterization of Sensors.

In order to use sensors to estimate Zn^{2+} concentrations, the apparent dissociation constants, K_d's, of the sensors must be determined. K_d's are typically quantified by purifying and titrating the sensors *in vitro*, and fitting the resulting data using the model developed by Grynkiewicz et al[13]. This model assumes a linear change of the emission intensity at both the donor FP and FRET emission wavelengths across all relevant analyte concentrations. Because this assumption is incorrect for many ratiometric sensors, different K_d's will be determined when the same dataset is plotted as the ratio of FRET emission over donor FP emission versus the inverse ratio.[8,14] Two models have been developed to determine more precise K_d's for ratiometric sensors. One method for fitting the *in vitro* data is to normalize the donor and/or FRET emission data using the emission intensity at the isosbestic point.[8] However, sensors that bind their analyte with cooperativity will not have an isosbestic point, so this method cannot be universally applied. A second protocol outlined by Pomorski et al.[14] calibrates the emission intensity data at both wavelengths yielding more precise K_d's, and can be applied to all sensors. This model was applied in this study.

To collect *in vitro* data, the sensors were titrated with a series of Zn^{2+} buffers at pH 7.4 and the intensities of the fluorescence emission were collected for the donor FP (λ_1 = 481 nm) and the acceptor FP (λ_2 = 529 nm). The ratio of the emission wavelengths (λ_2/λ_1) and inverse ratio (λ_1/λ_2) were plotted as a function of Zn^{2+} concentration (Supplementary Figure S7) and fit to determine the K_d of each sensor. Fits yielded K_d values within 1.7%. ZapCY1 can bind two Zn^{2+} so the data were fit with a model including the Hill coefficient (n) that gave a K_d = 17 pM and n = 0.47. This value indicates a slightly weaker sensor affinity for Zn^{2+} than the previously reported 2.5 pM.[1] Both eCALWY-4 and eZinCh-2 have one Zn^{2+} site and were fit with a model that excluded the Hill coefficient to give K_d = 164 pM and 103 pM, respectively. These values indicate that the sensors bind Zn^{2+} with a higher

affinity at pH 7.4 than pH 7.1 ($K_{d(eCALWY-4)}$ = 630 pM, $K_{d(eZinCh-2)}$ = 1000 pM), following the trend seen in these sensors' dissociation constants with increasing pH.[3,6]

Because ZapCY1 is fully saturated in the cytosol it cannot be used to estimate the cytosolic concentration of Zn^{2+}. Using K_d values and calibration data, the cytosolic Zn^{2+} concentrations were estimated to be 42 ± 2 pM (using eZinCh-2) and 133 ± 3 pM (using eCALWY-4). It should be noted that these numbers are the average and standard error when these equations are applied on a cell by cell basis, and do not include error from the K_d measurements which would increase the uncertainty in these numbers. In the ER, ZapCY1 estimates the concentration of labile Zn^{2+} to be 0.20 ± 0.04 pM, while ER-eCALWY-4 estimates a concentration of 49 ± 6 pM. ER-eZinCh-2 gives an estimate of labile Zn^{2+} in the ER of 70 ± 10 pM.

To better understand how oxidation might affect Zn^{2+} binding to the sensors in the ER, each sensor was purified and the FRET ratios in response to Zn^{2+} in the presence of tris(2-carboxyethyl)phosphine (TCEP), a reducing agent, and diamide, an oxidizing agent, were measured (Supplementary Table S4). All of the sensors responded to Zn^{2+} under reducing conditions. However, under oxidizing conditions the sensors were fluorescent but essentially non-responsive to Zn^{2+}. ZapCY1 appeared to be fixed in a high FRET state, with a FRET ratio similar to the R_{bound}. eZinCh-2 was fixed in a FRET state intermediate between R_{bound} and R_{apo}. Finally, eCALWY-4 exhibited an intermediate FRET ratio and responded slightly to Zn^{2+} but in the opposite direction of reduced sensor. In all cases, the presence of fluorescent but non-responsive sensor in cells may explain the decreased dynamic range of sensors in the ER of cells, as only a portion of the signal measured would be due to responsive FRET sensor.

Characterization of Sensor Affinity in Cells.

To determine if the oxidizing environment of the ER affects Zn^{2+} binding to the sensors, we estimated the apparent K_d of the sensors for Zn^{2+} directly in the ER. Previously, *in situ* titrations such as these were used to determine that the apparent K_d of a Zn^{2+} sensor in the cytosol closely matches the K_d determined with purified protein.[15] However, cysteine residues are known to undergo oxidative modifications that interfere with Zn^{2+} binding.[16] Furthermore, since immunoblots of the sensors indicate the formation of disulfide-linked oligomers and all three sensors feature oxidation-sensitive cysteine residues, it is possible that the environment of the ER might alter the binding properties of the sensors and result in systematic errors in measurements of Zn^{2+} concentration.

In situ titrations of ER-ZapCY1, ER-eZinCh-2, and ER-eCALWY-4 reveal that the apparent K_d in the ER is not significantly different than the K_d measured for purified protein. For the titrations, cells were treated with 50 μM TPEN and 1 μM thapsigargin to reach a stable R_{apo}, then treated with the optimized reagent conditions to reach a stable R_{zinc}. The sensors were tested with buffered Zn^{2+} solutions ranging from 2.5 pM to 2 nM labile Zn^{2+}. When saponin was excluded from the R_{zinc} solution, the sensors were unable to respond quickly enough for accurate measurements (Supplementary Figure S8). After addition of pyrithione, saponin, and buffered Zn^{2+}, cells were monitored until a stable signal was achieved.

The data were normalized to the TPEN-treated R_{apo} signal to visualize the magnitude of response to different buffered Zn^{2+} solutions (Figure 4, and raw data for these curves are presented in Supplementary Figures S9–11). Data from *in situ* titration experiments with all three sensors are plotted together as dynamic range versus Zn^{2+} concentration (Figure 4m). For ZapCY1 the sensor appears halfway saturated at 16 pM labile Zn^{2+}, which is consistent with the *in vitro* K_d. However, the steepness of this binding curve suggests that the cooperativity Zn^{2+} binding to ZapCY1 might be different in cells than in the test tube. Because of the low dynamic range of ER-eZinCh-2 and ER-eCALWY-4 the halfway saturation points of these sensors are more difficult to discern, but both are shifted in the direction of higher Zn^{2+} concentrations (39–72 pM) consistent with their higher *in vitro* K_d values. While the sensors undergo some oxidative modification and experience reduced dynamic range in the ER, the actual binding interaction between the sensors and Zn^{2+} ions does not appear to be significantly perturbed. Therefore, the *in vitro* measurements of K_d are still relevant in the ER.

Important Considerations for Applying FRET sensors to Subcellular Environments.

In this study we systematically examined the performance of three different Zn^{2+} sensor platforms to provide insight into the functionality of sensors in different environments within the cell. We demonstrate the importance of identifying optimal calibration conditions for accurately assessing the fractional saturation and Zn^{2+} concentration. Our finding that inclusion of saponin and use of low concentrations of buffered Zn^{2+} lead to more stable R_{bound} signals and larger dynamic ranges suggest that flooding cells with high concentrations of ions can yield sub-optimal calibrations. These reagents did not affect the pH or redox state of the ER (Supplementary Figures S12 and S13). This optimization of reagents has broad implications for calibration of other genetically encoded ion sensors, such as those for Ca^{2+}, Mg^{2+}, and Cu^{1+} where unstable bound signals are often observed.[17–19]

We also demonstrate that sensor performance can be adversely impacted by the oxidizing environment of the ER which can lead to formation of protein oligomers and reduced dynamic range. Although all three sensor platforms showed some degree of perturbation in the ER, as suggested by formation of disulfide linked oligomers and reduced dynamic range, the platforms were differentially affected. eZinCh2 was the most strongly perturbed (dynamic range reduced from 2.06 to 1.47, increase in variability in FRET ratio as measured by RCV from 5.1% to 32.4%, and perturbation of ER morphology in 25% of cells), perhaps due to surface exposed cysteine residues. eCALWY-4 was also perturbed, but to a lesser extent (dynamic range reduced from 1.83 to 1.32, but no change in variability in FRET ratio as measured by RCV: 26.5% vs 22.8% in cytosol and ER, respectively). Finally, ZapCY1 was the least perturbed in the ER environment (dynamic range reduced from 2.62 to 2.55, variability in FRET ratio increased from 9.3% to 11.1% in the cytosol versus ER, respectively). Despite some degree of perturbation in the ER environment, the estimated K_d values for each sensor closely matched the *in vitro* measurements. Combined, these results suggest that eCALWY-4 and ZapCY1 are more suitable than eZinCh-2 to estimate relative amount of ER Zn^{2+}, and of the two sensor platforms ZapCY1 has a higher dynamic range and less evidence of perturbation.

When calibrated using the new conditions identified here, ZapCY1 and eCALWY-4 both have lower fractional saturation in the ER than in the cytosol. Since the apparent K_d of the sensors for Zn^{2+} was not altered in the ER, this decrease in fractional saturation of the sensors supports the conclusion that labile Zn^{2+} levels in the ER are lower than cytosolic levels. However, it is important to note that our study does not exclude the possibility that ER Zn^{2+} could be higher in different types of cells or that changes in cellular state due to signaling could generate a pool of labile ER Zn^{2+}. The higher dynamic range of ER-ZapCY1 allows for more accurate quantification and detection of small changes in labile Zn^{2+} in the ER.

This study sought to establish performance metrics for genetically encoded FRET sensors, demonstrating the importance of optimal *in situ* calibration conditions, measurement of accurate K_d values using the method of Pomorski et al[14], comparison of K_d values *in vitro* and in organelle-targeted locations, and use of a new microfluidic platform to assess sensor performance and variability in thousands of cells. We reveal that simply targeting a sensor to a particular organelle is not sufficient to guarantee effective performance. Instead, it is important to rigorously examine how performance might be affected by the organelle environment. Our study reveals that different sensor platforms are differentially impacted by organelle environments, suggesting the need for approaches to systematically optimize sensor performance in the desired subcellular location.

METHODS

Details of chemicals, cloning, cell culture, microscope settings, microfluidic experiments, immunoblots, protein purification and in vitro characterization are provided in the Methods section of Supporting Information.

Reagent optimization experiments.

HeLa cells ($n \geq 3$ cells for every experiment) were treated with 50 μM TPEN (cytosolic sensors) or 50 μM TPEN with 1 μM thapsigargin (ER sensors) for 40 min prior to imaging. R_{apo} data was collected, then cells were washed with phosphate, calcium, and magnesium-free HEPES-buffered HBSS, pH = 7.4 to remove the chelate and then treated with pyrithione and Zn^{2+} with or without saponin. Data was normalized to R_{apo} by dividing the FRET ratio (R) throughout the experiment by the average R_{apo} value (R/R_{apo}). Normalized data is presented as the average normalized FRET ratio of at least three cells.

Calibration and *in situ* titration experiments.

To collect $R_{resting}$ data for calibration experiments, cells ($n \geq 3$ cells for every experiment) were imaged in phosphate-free HEPES-buffered HBSS, pH 7.4 to prevent Zn^{2+} precipitation. To collect R_{apo} data, cells were treated with 50 μM TPEN (cytosolic sensors) or 50 μM TPEN with 1 μM thapsigargin, (ER sensors, thapsigargin was previously shown to help deplete ER of Zn^{2+1}) until a stable signal was achieved. Cells were then washed with phosphate, calcium, and magnesium-free HEPES-buffered HBSS, pH = 7.4 to remove the chelate and then treated with pyrithione and Zn^{2+} with or without 0.001% (w/v) saponin. For *in situ* titrations, data was normalized to R_{apo} for each of the sensors as follows: ER-

ZapCY1 ($R–R_{apo}$) or ER-eCALWY ($1–(R_{apo}–R)$). Normalized data is presented as the average normalized FRET ratio of at least three cells.

Data Analysis.

All imaging data were analyzed in MATLAB (Mathworks). Images were background corrected by drawing a region of interest (ROI) in a blank area of the image and subtracting the average fluorescence intensity of the background ROI from the average intensity of each cell. FRET ratios for each cell were calculated by dividing the background-corrected YFP FRET intensity by the background-corrected CFP intensity ($(I_{cellular\ FRET} - I_{background\ FRET})/(I_{cellular\ CFP} - I_{background\ CFP})$). Unless indicated otherwise, error bars are standard error of the mean.

Supplementary Material

Refer to Web version on PubMed Central for supplementary material.

ACKNOWLEDGMENTS

We thank T. Nahreini for assisting the cell culture and flow cytometry analysis, J. Dragavon for microscopy assistance and advice, and L. Sanford for help writing analysis scripts in MATLAB.

Funding

We would like to acknowledge the following sources for generous financial support: NIH GM084027 and DP1-GM114863 (to A.E.P.), NIH T32 GM008732 (to K.P.C). This work was supported by the NSF Physics Frontier Center at JILA (NSF PHY 1125844, to R.J.). R.J. is a staff member in the Quantum Physics Division of the National Institute of Standards and Technology (NIST). Certain commercial equipment, instruments, or materials are identified in this paper in order to specify the experimental procedure adequately. Such identification is not intended to imply recommendation or endorsement by the NIST, nor is it intended to imply that the materials or equipment identified are necessarily the best available for the purpose.

References

(1). Qin Y, Dittmer PJ, Park JG, Jansen KB, Palmer AE. Proc. Natl. Acad. Sci. U. S. A. 2011; 108(18): 7351. [PubMed: 21502528]

(2). Vinkenborg JL, Nicolson TJ, Bellomo EA, Koay MS, Rutter GA, Merkx M. Nat Meth. 2009; 6(10):737.

(3). Hessels AM, Chabosseau P, Bakker MH, Engelen W, Rutter GA, Taylor KM, Merkx M. ACS Chem. Biol. 2015; 10(9):2126. [PubMed: 26151333]

(4). Park JG, Qin Y, Galati DF, Palmer AE. ACS Chem. Biol. 2012; 7(10):1636. [PubMed: 22850482]

(5). Miranda JG, Weaver AL, Qin Y, Park JG, Stoddard CI, Lin MZ, Palmer AE. PLoS One. 2012; 7(11):e49371. [PubMed: 23173058]

(6). Chabosseau P, Tuncay E, Meur G, Bellomo EA, Hessels A, Hughes S, Johnson PRV, Bugliani M, Marchetti P, Turan B, Lyon AR, Merkx M, Rutter GA. ACS Chem. Biol. 2014; 9(9):2111. [PubMed: 25011072]

(7). Qin Y, Miranda JG, Stoddard CI, Dean KM, Galati DF, Palmer AE. ACS Chem. Biol. 2013; 8(11): 2366. [PubMed: 23992616]

(8). Hessels AM, Merkx M. ACS Sensors. 2016; 1(5):498.

(9). Fiedler BL, Van Burskirk S, Carter KP, Qin Y, Carpenter MC, Palmer AE, Jimenez R. Anal. Chem. 2017; 89(1):711. [PubMed: 27959493]

(10). (ParkJG; PalmerAE, ZhangJ, NiQ, NewmanHR, Eds.; Humana Press: Totowa, NJ, 2014; pp 29–47.

(11). Ma H, Gibson EA, Dittmer PJ, Jimenez R, Palmer AE. J. Am. Chem. Soc. 2012; 134:2488. [PubMed: 22260720]

(12). Costantini LM, Baloban M, Markwardt ML, Rizzo M, Guo F, Verkhusha V, Snapp V. E. L. Nat Commun. 2015:6.

(13). Grynkiewicz G, Poenie M, Tsien RY. J. Biol. Chem. 1985; 260(6):3440. [PubMed: 3838314]

(14). Pomorski A, Kochańczyk T, Miłoch A, Krężel A. Anal. Chem. 2013; 85(23):11479. [PubMed: 24180305]

(15). Dittmer PJ, Miranda JG, Gorski JA, Palmer AE. J. Biol. Chem. 2009; 284(24):16289. [PubMed: 19363034]

(16). Maret W, Li Y. Chem. Rev. 2009; 109(10):4682. [PubMed: 19728700]

(17). Palmer AE, Giacomello M, Kortemme T, Hires SA, Lev-Ram V, Baker D, Tsien RY. Chem. Biol. 2006; 13(5):521. [PubMed: 16720273]

(18). Lindenburg LH, Vinkenborg JL, Oortwijn J, Aper SJA, Merkx M. PLoS One. 2013; 8(12):e82009. [PubMed: 24312622]

(19). Wegner SV, Arslan H, Sunbul M, Yin J, He C. J. Am. Chem. Soc. 2010; 132(8):2567. [PubMed: 20131768]

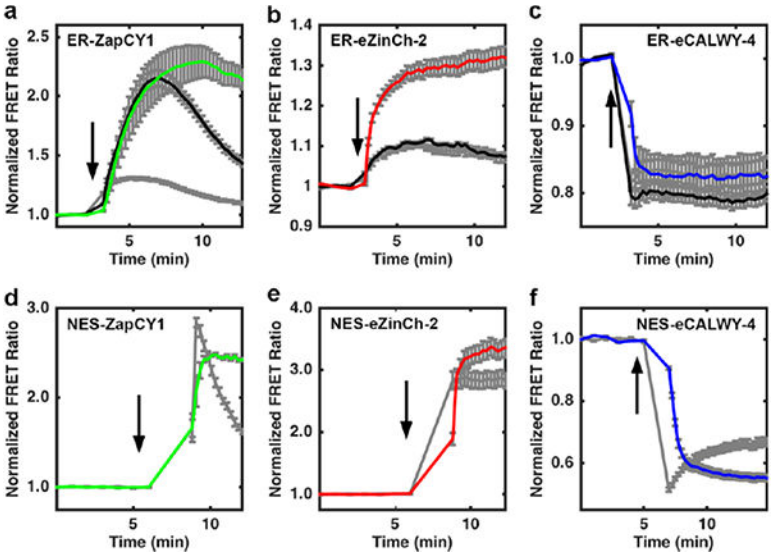

Figure 1.

Optimization of zinc conditions for ER (a-c) and NES (d-f) sensors: ZapCY1 (green), eZinCh-2 (red), eCALWY-4 (blue). Arrows indicate washing of cells followed by addition of solutions containing 100 μM $ZnCl_2$ + 5 μM pyrithione (grey lines), 2 nM buffered Zn^{2+} + 0.75 μM pyrithione (black lines, not done for NES sensors (d-f)), or 2 nM buffered Zn^{2+} + 0.75 μM pyrithione + 0.001% (w/v) saponin (lines in color) to cells treated for 40 minutes with 50 μM TPEN. Raw FRET ratios are provided in Figure S1.

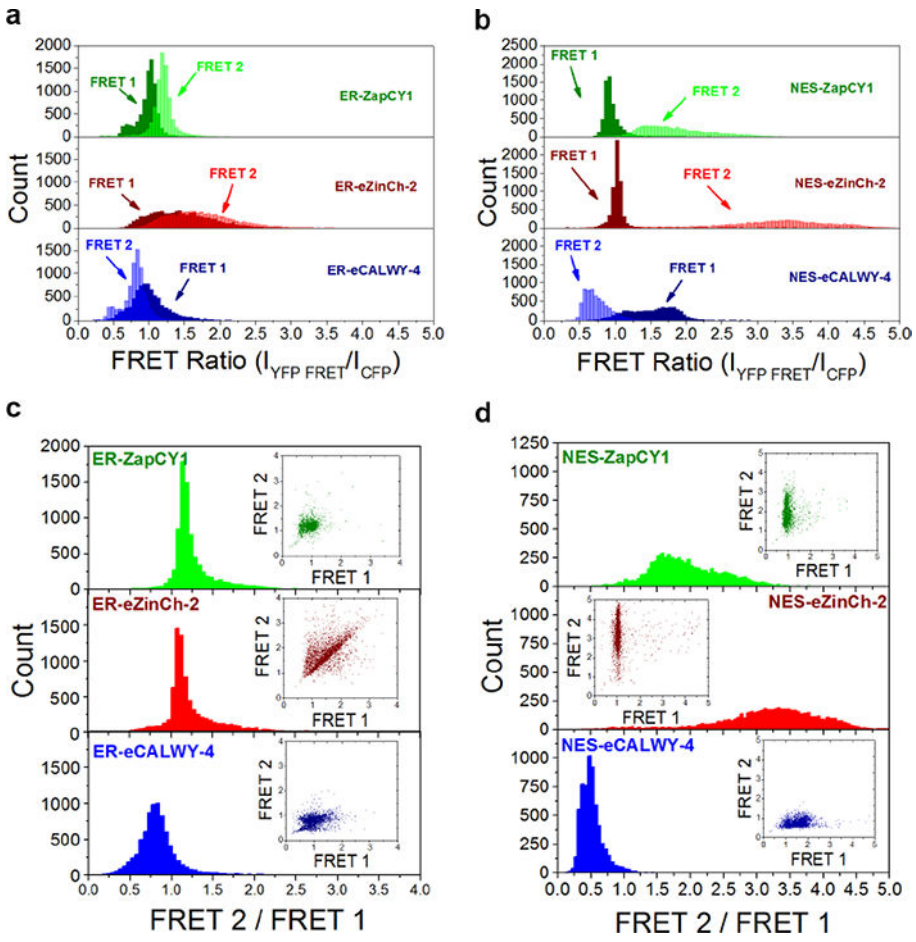

Figure 2:

Microfluidic analysis of FRET sensor response. FRET ratio histograms for HeLa cells expressing ER (a) or cytosol (b) targeted sensors indicating FRET 1 and FRET 2 cell populations. Corresponding pairmatched FRET ratio histograms showing FRET response to pyrithione and Zn^{2+} for ER (c) and cytosol (d) targeted sensors. Inset scattergrams show FRET response on the single cell level. Time delay between FRET 1 and FRET 2 for all data shown is 7.5 seconds. Sample size for each plot is 6500 cells.

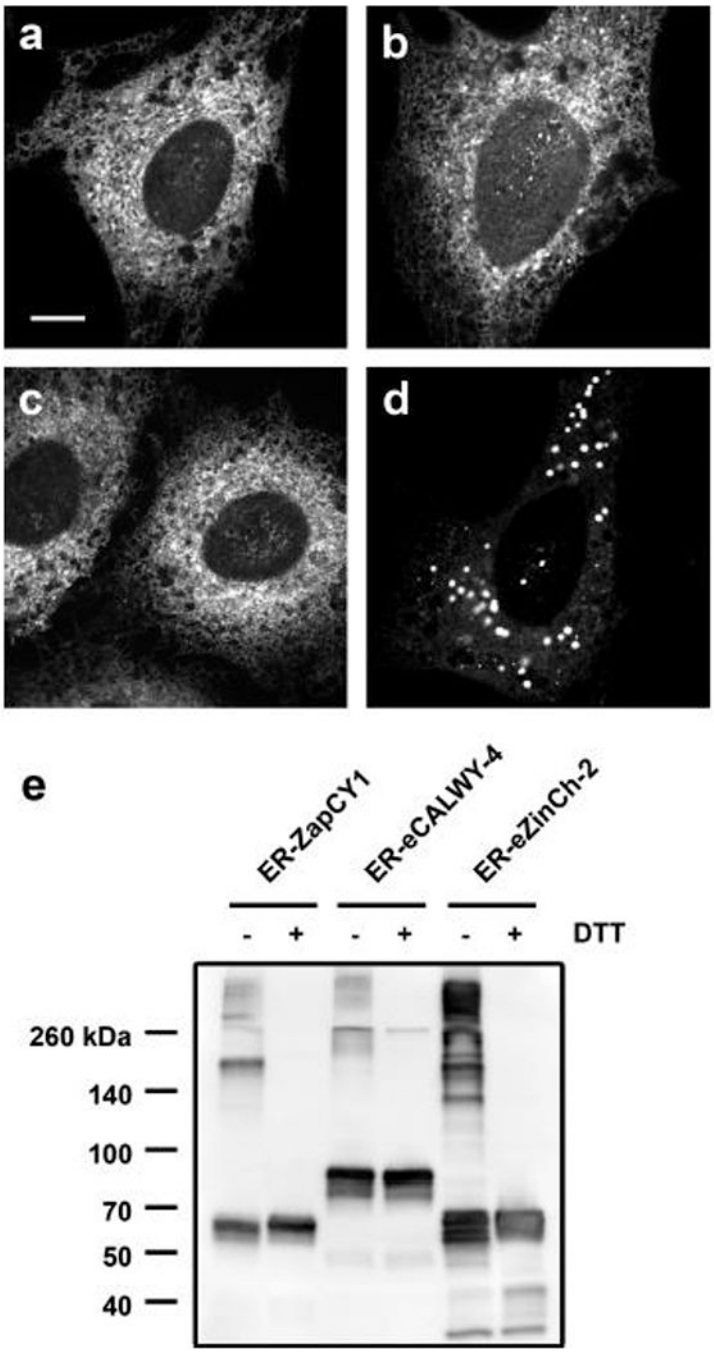

Figure 3.

Measurement of localization to and aggregation in the ER. ER-ZapCY1 (a) and ER-eCALWY-4 (b) localize properly to the ER. Some cells expressing ER-eZinCH-2 have proper localization (c) but approximately 25% of cells exhibit bright puncta (d) regardless of signal sequence used (Figure S4). Western blot (e) of sensors in the ER under non-reducing and reducing conditions (denoted by – or + DTT) reveals that all sensors form DTT-sensitive oligomers.

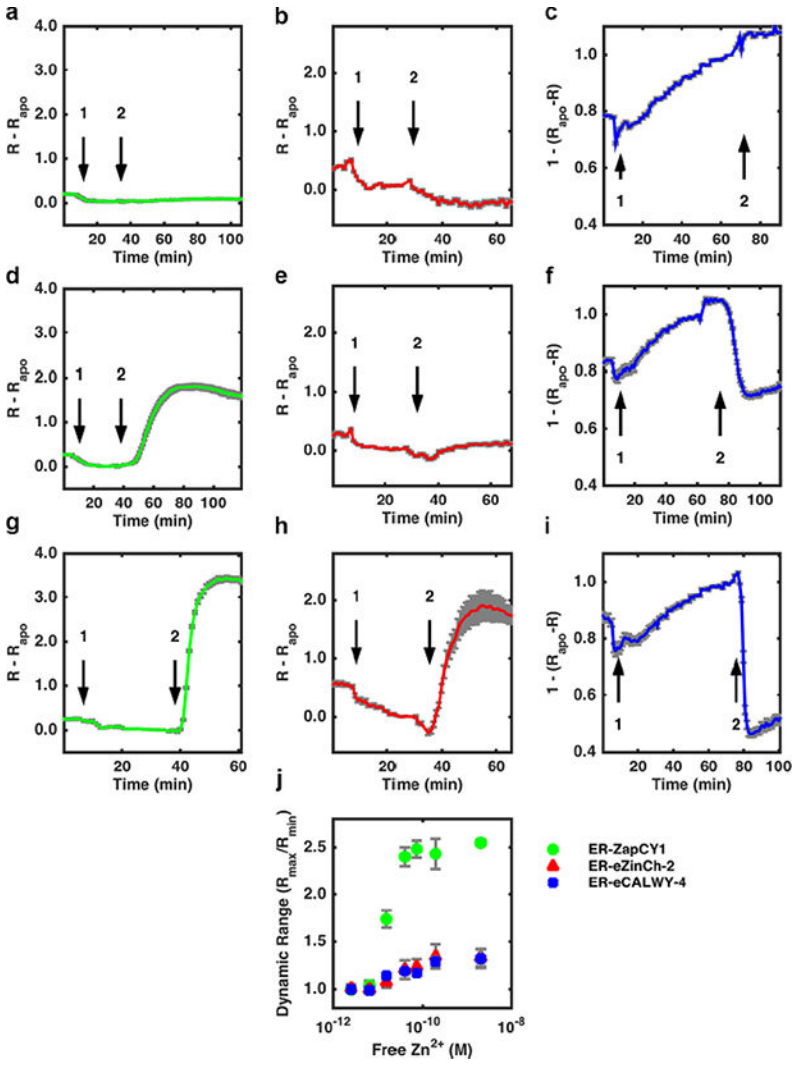

Figure 4.

In situ titrations of ER-targeted zinc sensors ZapCY1 (a, d, g), eZinCh-2 (b, e, h), and eCALWY-4 (c, f, i). Arrows marked (1) indicate addition of 50 μM TPEN + 1 μM thapsigargin to cells. Arrows marked (2) indicate washing out of TPEN and addition of buffered Zn^{2+} + 0.75 μM pyrithione + 0.001% (w/v) saponin to cells. Cells were treated with 6.6 pM (a-c), 16 pM (d-f), or 192 pM (g-i) buffered Zn^{2+} solutions. Plots of dynamic range for ER-ZapCY1, eZinCh-2, and ER-eCALWY-4 over Zn^{2+} concentration suggest that Zn^{2+} binding by the sensors in not drastically altered in the ER (j). Each data point is the average dynamic range and standard error of the mean from a-i. Data for 2 nM Zn^{2+} data point is from Figure 2. Raw FRET ratios and additional data are provided in Figures S8–10.

Table 1.

Fractional saturation and dynamic range of ER- and cytosol-targeted Zn^{2+} sensors.

	ZapCY1		eZinCh-2		eCALWY-4	
	Fractional Saturation	Dynamic Range	Fractional Saturation	Dynamic Range	Fractional Saturation	Dynamic Range
ER	4.7 ± 0.4%	2.55 ± 0.02	40 ± 4%	1.47 ± 0.04	21 ± 2%	1.32 ± 0.04
Cytosol	100%	2.62 ± 0.05	33.2 ± 0.8%	2.06 ± 0.06	39.6 ± 0.6%	1.83 ± 0.04